Document Version: Accepted author manuscript. Link to publication record in Manchester Research Explorer
DOI: 10.1109/TIA.2022.3185571

A Fast 3-D Winding Inductance Estimation Method for Air-Cored Resonant Induction Machines

Zhao Jin, Matteo F. Iacchetti, *Senior Member, IEEE*, Alexander C. Smith, *Senior Member, IEEE*, Rajesh P. Deodhar, *Senior Member, IEEE*, Yoshiyuki Komi, *Member, IEEE*, Ahmad Anad Abduallah, *Student Member, IEEE*, Chiaki Umemura

***Abstract*—The air-cored resonant induction machine removes the magnetic core so the fields produced by the windings are truly 3-D in nature. The end-windings normally regarded as a non-active and leakage source in conventional iron-cored machines now become an active part and contribute to the torque production. Therefore, the electromagnetic modeling can no longer be reduced to a 2-D analysis and the 3-D inductance calculation becomes a key problem. The 3-D Finite Element Analysis (FEA) can solve the 3-D magnetic field but, firstly, the validity of its solution depends on the precision in geometry modeling. In particular, representing the end-winding region avoiding conductor clashing can be very complicated. Secondly, 3-D FEA solutions are computationally-slow and therefore inefficient as an "internal routine" of an optimization procedure. This paper proposes a fast analytic 3-D winding inductance estimation method for air-cored resonant induction machines. The approach breaks down the real coils into straight conductors and represents them by single filaments located at their centers, then uses closed-form expressions derived from Neumann integrals to calculate the coil self and coil-to-coil mutual inductances which are then collected into winding phase self and mutual inductances. All the independent coil-pair contributions are isolated so as to eliminate redundant calculations. Good accuracy of the calculated results is confirmed by validation against both 3-D FEA and experimental results, including winding inductance breakdown and overall machine tested performance.**

***Index Terms*—Air-cored windings, closed-form expressions, collection routine, experimental validation, inductance calculation, resonance.**

I. Introduction

REMOVING the ferromagnetic core from conventional induction machines (IMs) significantly reduces the weight, eliminates iron losses and magnetic saturation. However, it also reduces the air-gap flux density. In order to maintain the power rating, capacitors are added to cancel out the machine inductive reactance and achieve resonance at a certain slip so that the electric loading is boosted for a given voltage. This is the main idea behind air-cored resonant induction machines (ACRIMs) [1]. The concept was firstly proposed in [2]. The performance analysis, including torque and efficiency calculations, can be carried out using the standard per-phase equivalent circuit, where the key parameters are the inductance and capacitance values. Several tuning criteria for the capacitors have been discussed and compared in [3] and [4], but the calculation of air-cored IM inductances has not been studied thoroughly in previous works. Analytic expressions for the inductances of ACRIMs can be found in [5] and [6], but they are derived under the assumption of two-dimensional (2-D) current sheet distributions or using the 2-D field solution of wires with round cross-sections, none of them is based on three-dimensional (3-D) models, and therefore are not accurate for an air-cored machines. The Finite Element Analysis (FEA) method is used in [7] and [8] to extract ACRIM inductance values but it is still based on a 2-D model, so does not capture the important 3-D effects.

The inductance estimation for ACRIMs is inherently a 3-D magnetic problem: similar problems can be found in end-winding leakage reactance calculation, ironless permanent magnet (PM) machine design, air-cored compulsator design, etc. Various methods have been proposed in the literature. To calculate the end-winding reactance of induction machines, 3-D FEA models are built in [9] and [10]. However, solving these 3-D FEA models is quite time-consuming. In order to reduce the computation time, a method using partial 3-D FEA models and a corrected 2-D FEA model is proposed in [11]. This method achieves very close accuracy to a full 3-D FEA with reduced computational solution times, but when the machine parameters change, the winding geometry needs to be adjusted accordingly to avoid coils clashing and the boundary conditions also need to be reassigned. 3-D FEA is also incorporated to calculate the machine inductance and back-emf in the design optimization for an axial-flux PM generator with an ironless stator in [12]. However, the results show that running a parametric sweep takes about 92 hours on a high-performance workstation. In summary, although 3-D FE modelling can be a way to numerically calculate the inductances, the complexity of the coil arrangements in the end-regions and the high computational cost makes it very inefficient for optimization design procedures.

Compared to 3-D-FEA numerical methods, analytical methods and hybrid numerical-analytical methods can reduce the computational burden and achieve good accuracy [13] – [16]. Neumann integrals are implemented in [17] to calculate

Zhao Jin and Alexander C. Smith are with the Department of Electrical and Electronic Engineering, The University of Manchester, Manchester, M13 9PL, U.K. (e-mail: zhao.jin@manchester.ac.uk; sandy.smith@manchester.ac.uk).

Matteo F. Iacchetti is with the Department of Energy, Politecnico di Milano, via Lambruschini 4, 20156 Milan, Italy, and also with the Department of Electrical and Electronic Engineering, The University of Manchester, Manchester, M13 9PL, U.K. (email: matteo.iacchetti@manchester.ac.uk).

Rajesh P. Deodhar and Ahmad Anad Abduallah are with the IMRA Europe S.A.S. UK Research Centre, Brighton, BN1 9RS, U.K. (e-mail: rd@imra-ukrc.com; aa@imra-ukrc.com).

Yoshiyuki Komi and Chiaki Umemura are with the Aisin Corporation, 448-8650 Kariya, Japan (e-mail: yk@imra-ukrc.com; cu@imra-ukrc.com).

the end-winding inductance for concentrically-wound IMs: coils are represented by their central filaments, and a coil table is used to store the information such as the coil winding direction and coil connections. However, the direct implementation of Neumann integrals via numeric quadrature can produce a singularity if any two elements intersect which prevents end-winding shape simplification, and, although it is significantly faster than 3-D FEA, it can still be too slow as the "inner core" of fast design optimization procedures. Hence, closed-form solutions of Neumann integrals are derived in [18] and [19] for mutual inductances of two straight filaments placed in an arbitrary position and of two parallel and coaxial rectangular loops. Coils can be approximated by small straight segments and assumed to have a round cross-section in the self-inductance calculation and point cross-section in the mutual inductance calculation [18]. For the mutual inductances between more complex shapes such as arc filaments and coaxial circular filaments, solving Neumann integrals can yield expressions involving asymptotical series approximation and elliptic integrals, so hybrid numerical-analytical evaluation is needed [20] – [22]. The closed-form expressions exhibit good accuracy, resolve singularity issues and can be computed quickly on standard computers [23]. However, most papers focus on the coil-level inductance calculation while the winding-level inductance collection is ignored. Due to the properties of a three-phase winding layout, periodicity and symmetry can be invoked to enable a faster winding inductance collection which further reduces the computation time and is suitable for a 3-D optimization design program.

This paper proposes a fast winding estimation method for ACRIMs. Coils are initially broken down into straight conductors and a single filament located at the center of each conductor is used to represent coil shape and position. Closed-form solutions are then derived from Neumann integrals to calculate the self and mutual inductances of these straight segments with arbitrary orientation, which avoids singularity issues and accelerate calculation times. Segment-level inductances are then summed to obtain the coil self and coil-to-coil mutual inductances. The coil-level inductances are subsequently collected to calculate the phase self and phase-to-phase mutual inductances, so that only independent coil-pairs are involved, which eliminates redundant computation and further reduces the computation burden. Finally, the phase self and phase-to-phase mutual inductances are combined into the equivalent-circuit per-phase inductances. The proposed method is validated against 3-D FEA. Compared to [1], this paper also adds an experimental validation on an ACRIM prototype: the determination of the coil shape using measurable prototype geometric parameters is presented, from which the estimated winding inductance values are calculated then compared with the measured values. The estimation accuracy is also validated in the comparison between the analytically-predicted and tested ACRIM performance.

II. Coil Inductance

A. Inductances of Straight Conductors

In the analytic estimation, coils are assumed to be composed of straight conductors with a round cross section. The first step to work out coil inductances is to determine the self-inductance of one segment and the mutual inductance of a pair of segments with arbitrary orientation. Closed-form solutions for Neumann integrals were developed in [23], their expressions are very convoluted so will not be repeated here.

1) Self-Inductance of a Straight Conductor

The formal expression for the self-inductance of a nonmagnetic, straight conductor can be written as

$$L_{cond} = f_L(l, \rho) \tag{1}$$

where l is the conductor length, ρ is the radius of its cross section.

2) Mutual Inductance of Two Straight Conductors

Representing the conductors by straight filaments locating at their centers, the mutual inductance of a pair of conductors can be expressed as follows:

$$M_{cond} = f_M(P_1, Q_1, P_2, Q_2) \tag{2}$$

where $\{P_1,Q_1\}$ and $\{P_2,Q_2\}$ are the coordinates of the start and end points of filaments 1 and 2 respectively. The spatial relationship of the two filaments is firstly determined using the coordinates of P_1, Q_1, P_2, Q_2, then for different filament orientations, such as parallel, skew, meeting at one end, intersecting, etc., different closed-form expressions are applied. For reinforced robustness, if two filaments intersect, they can also be broken down at the intersection point and their mutual inductance can be treated as the sum of mutual inductances of several sub-filaments meeting at one end. This approach resolves any singularity issue arising from the intersection of filaments.

Comparison of the analytic results with numeric integrals shows that, the closed-form expressions are accurate, robust and computationally fast, and therefore suitable to be integrated into optimization design programs.

B. Self-Inductance of a Coil

Assuming the coil is composed of N straight segments, the self-inductance of the coil is

$$L_{coil} = \sum_{i=1}^{N}\left(L_i + \sum_{j=1,\, j\neq i}^{N} M_{ij} \right) \tag{3}$$

where L_i is the self-inductance of i-th segment, M_{ij} is the mutual inductance between the i-th and the j-th ($i \neq j$) segments.

C. Mutual Inductance of a Pair of Coils

Supposing the coil 1 and coil 2 are composed of N_1 and N_2 straight segments respectively. The mutual inductance between two coils is

$$M_{coil} = \sum_{i=1}^{N_1}\sum_{j=1}^{N_2} M_{ij} \tag{4}$$

where M_{ij} is the mutual inductance between the i-th segment from coil 1 and the j-th segment from coil 2. In a radial-flux machine, stator and rotor coils are typically located on two concentric baseline circles of radii r_{b1} and r_{b2}, as shown in Fig. 1. When the coil geometries and the radii of the baseline

circles are fixed, the mutual position of the coils is defined by the angle $\Delta\theta$ between the two coil axes. As a result, the mutual inductance of a pair of coils can be written as

$$M_{coil} = M(\Delta\theta) \tag{5}$$

which is a function of the angle between the two coils.

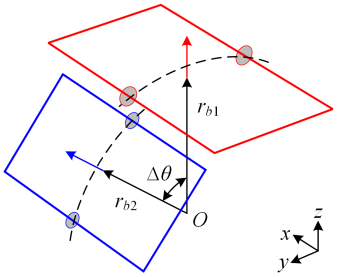

Fig. 1. A pair of coils (solid thick lines) on two concentric baseline circles (dashed lines) of radii r_{b1} and r_{b2}. The grey circles represent the cross-sections of the coils. The angle between two coil (magnetic) axes is $\Delta\theta$.

III. Phase Winding and Equivalent-Circuit Inductance Collection Routine

The next step is to group the individual coil inductances to form the phase winding self and mutual inductances. Balanced three-phase, single-layer, lap windings are assumed for the stator and rotor with each winding composed of identical coils with appropriate connections. Stator and rotor coils are different, lying on concentric baseline circles of different radii (see Fig. 1). The winding layout has periodicity p_p however, where p_p is the number of pole pairs, this property can be used to reduce the number of calculations for coil-to-coil inductances.

A. Phase Self-Inductance

The self-inductance, L_{ph}, of the stator or rotor phase winding (i.e., with identical coils on the same baseline circle) can be divided into three parts,

$$L_{ph} = L_0 + M_1 + M_2 \tag{6}$$

where L_0 is the sum of self-inductances of all coils in the phase, M_1 is the sum of mutual inductances between coils in the same phase and same pole pair, M_2 is the sum of mutual inductances between coils in the same phase but different pole pairs.

1) Term L_0

Because coils are identical, the sum of self-inductances of all coils in a phase is

$$L_0 = p_p q L_{coil} \tag{7}$$

where q is the number of coils per pole per phase, L_{coil} is the self-inductance of one single coil. The number of coil inductance calculations involved in L_0 is $n_0 = 1$.

2) Term M_1

Coil pairs with the same coil angular distance $\Delta\theta$ produce identical contributions, so their mutual inductances only need to be calculated for independent, i.e., not repeated, coil pairs and then multiplied by their number of repetitions. This approach eliminates redundancy and accelerates the calculation.

Based on the slot numbering shown in Table I, the coil angular distances and their numbers of repetitions are summarized in Table II. It can be seen that, when $q > 1$, there are $2p_p(q-i)$ coil pairs with $\Delta\theta = i\alpha$, where α is the angle between the geometric axes of two coils and plays the role of a "slot angle".

Table I
The Slot Numbering

Pole pair number	Phase band	Slot number
1	A	1, 2, …, q
	$\bar{B}$	q+1, …, 2q
	C	2q+1, …, 3q
	$\bar{A}$	3q+1, …, 4q
	B	4q+1, …, 5q
	$\bar{C}$	5q+1, …, 6q
⋮	⋮	⋮

Table II
Angular Distances Between Coils in the Same Phase and Same Pole Pair, and the Number of Repetitions *

$\Delta\theta$	Number of repetitions
α	$2p_p(q-1)$
2α	$2p_p(q-2)$
…	…
$i\alpha$	$2p_p(q-i)$
…	…
$(q-1)\alpha$	$2p_p$

* $q \geq 2$. $1 \leq i \leq q-1$

The sum of mutual inductances between coils in the same phase and same pole pair can be written as,

$$M_1 = \begin{cases} 2p_p \sum_{i=1}^{q-1} (q-i) M(i\alpha) & \text{if } q \geq 2 \\ 0 & \text{if } q = 1 \end{cases} \tag{8}$$

The number of calculations for independent coil pairs is $n_1 = q-1$.

3) Term M_2

It can be seen from Fig. 2 that, the sum of mutual inductances between coils from pole pairs 1 and 2+j is identical to the sum of mutual inductances between coils from pole pairs 1 and p_p-j ($0 \leq j \leq p_p-2$) when $p_p > 2$. This property can be invoked along with periodicity to avoid repeating calculations between every two pole pairs.

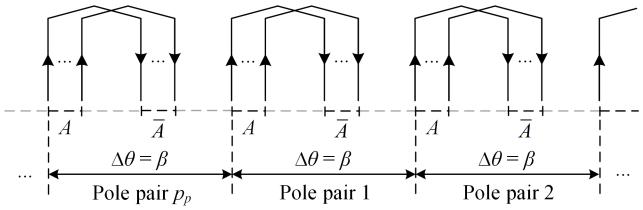

Fig. 2: The winding layout for the coils in the same phase but different pole pairs ($p_p \geq 3$), where β is the pole-pair angular span and only coils in phase A are shown. The sum of mutual inductances between coils from pole pairs 1 and 2 is identical to the sum of mutual inductances between coils from pole pairs 1 and p_p, and so on.

Also, based on Table I, the coil distances and their repetitions are summarized in Table III, where β is the pole-pair angular span.

The sum of mutual inductances between coils in the same phase but different pole pairs is

$$M_2 = \begin{cases} p_p\left(2\sum_{j=1}^{K} S(j) + Z\right) & \text{if } p_p \geq 3 \\ p_p Z & \text{if } p_p = 2 \\ 0 & \text{if } p_p = 1 \end{cases} \quad (9)$$

where the expressions for S, Z and K are presented in the Appendix. The number of calculations for independent coil pairs involved in M_2 is

$$n_2 = \begin{cases} \frac{p_p - 1}{2}(2q-1) & \text{if } p_p \text{ is odd} \\ \frac{p_p}{2}(2q-1) & \text{if } p_p \text{ is even} \end{cases} \quad (10)$$

The total number of coil self-inductance and coil-to-coil mutual inductance calculations in the phase winding self-inductance collection is $n_{Lph} = n_0+n_1+n_2$.

Table III
Angular Distances Between Coils in the Same Phase but Different Pole Pairs and the Number of Repetitions *

$\Delta\theta$	Number of repetitions
$(j-1)\beta$	$p_p q$
$(j-1)\beta\pm\alpha$	$p_p(q-1)$
...	...
$(j-1)\beta\pm i\alpha$	$p_p(q-i)$
...	...
$(j-1)\beta\pm(q-1)\alpha$	p_p

* $q \geq 1$, $p_p \geq 2$. $1 \leq i \leq q-1$ when $q \geq 2$, $2 \leq j \leq p_p$.

B. Mutual Inductance of Two Adjacent Phases on the Same Baseline Circle

For a balanced three-phase winding, the mutual inductances between two adjacent phases are identical, i.e., $M_{AB} = M_{BC} = M_{CA}$. Based on Table I, the angular distances between coils from two adjacent phases and their number of repetitions can be summarized as shown in Table IV.

Table IV
Angular Distances Between Coils from Two Adjacent Phases and the Number of Repetitions *

$\Delta\theta$	Number of repetitions
$(j-1)\beta+2q\alpha$	$p_p q$
$(j-1)\beta+(2q\pm1)\alpha$	$p_p(q-1)$
...	...
$(j-1)\beta+(2q\pm i)\alpha$	$p_p(q-i)$
...	...
$(j-1)\beta+(2q\pm(q-1))\alpha$	p_p

* $q \geq 1$, $p_p \geq 1$. $1 \leq i \leq q-1$ when $q \geq 2$, $1 \leq j \leq p_p$.

Then the mutual inductance of two adjacent phases on the same baseline circle, M_{ph}, can be written as

$$M_{ph} = \begin{cases} p_p \sum_{j=0}^{p_p-1} \left(qM(j\beta + 2q\alpha) \right. & \\ \left. + \sum_{i=1}^{q-1} (q-i)M(j\beta + (2q \pm i)\alpha)\right) & \text{if } q \geq 2 \\ p_p \sum_{j=0}^{p_p-1} M(j\beta + 2q\alpha) & \text{if } q = 1 \end{cases} \quad (11)$$

The number of calculations for independent coil pairs is $n_{Mph} = p_p(2q-1)$.

C. Mutual Inductance of Two Phases on Two Different Baseline Circles

The number of stator and rotor coils per pole per phase are denoted as q_s and q_r respectively. The stator and rotor have the same angular pole-pair span, $\beta = 2\pi/p_p$. Fig. 3a shows the stator and rotor slots when the first coils of the stator phase A and rotor phase a are geometrically aligned to each other. The corresponding rotor position is defined as origin for the rotor rotation angle. Assuming that the phase sequence of the windings for both stator and rotor is "$A\bar{B}C\bar{A}B\bar{C}$ (repeated) ...", when the rotor rotates by an arbitrary angle φ, as shown in Fig. 3b, the position for every coil in the stator reference frame can be derived as shown in Table V.

The origin for coil position, $\theta = 0$, is defined as the coil axis position of the first coil in stator phase A in pole pair 1. Angle $\theta_A(i_s,j_s)$ refers to the position of i_s-th coil of phase A in j_s-th pole pair measured from the assumed origin for θ. Based on the coil positions, the angle between any two coils can be calculated. For example, the angle between coil (i_s,j_s) in stator phase A and coil (i_r,j_r) in rotor phase a is $\Delta\theta_{Aa}(i_s,j_s,i_r,j_r) = \theta_a(i_r,j_r) - \theta_A(i_s,j_s)$, and the sum of all $M(\Delta\theta_{Aa}(i_s,j_s,i_r,j_r))$ yields the mutual inductance between stator phase A and rotor phase a. In summary, the mutual inductance between one stator phase winding and one rotor phase winding when the rotor is at a generic position φ is (12).

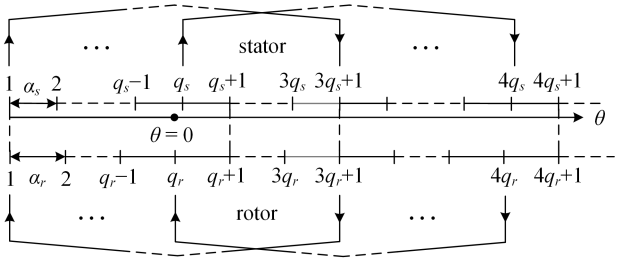

(a)

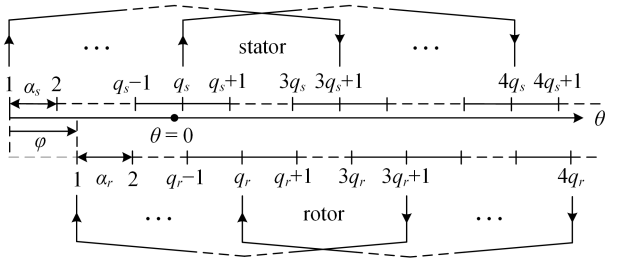

(b)

Fig. 3: (a) Stator (top) and rotor (bottom) coil slots (= ticks) when the first (= label "1") stator and rotor coils of phases A and a are geometrically aligned. (b) The rotor rotates by an angle φ.

$$M_{sr}(\varphi) = p_p \sum_{j=0}^{p_p-1} \sum_{i=0}^{q_s-1} \sum_{k=0}^{q_r-1} M(\Delta\theta(i,j,k,\varphi)) \quad (12)$$

where

$$\Delta\theta(i,j,k,\varphi) = j\beta - i\alpha_s + (uq_r + k)\alpha_r + \varphi \quad (13)$$

The number of calculations for independent coil pairs is

$n_{sr} = p_p q_s q_r$. The mutual inductance between stator phase *A* winding and rotor phase *a* winding at a generic rotor position, i.e., $M_{Aa}(\varphi)$, is when u in (13) is set to 0, $M_{Ab}(\varphi)$ is when $u = 4$, and $M_{Ac}(\varphi)$ is when $u = 2$. Other stator-to-rotor phase mutual inductances can be directly written by invoking cyclic symmetry. Therefore, at any rotor rotation angle, $M_{Aa} = M_{Bb} = M_{Cc}$, $M_{Ab} = M_{Bc} = M_{Ca}$, and $M_{Ac} = M_{Cb} = M_{Ba}$.

Table V
Angular Position of *i*-th Coil in *j*-th Pole Pair in all Stator and Rotor Phases *

Phase	Angular position of coil (*i*,*j*)
Stator, *A*	$\theta_A(i_s,j_s)=(j_s-1)\beta+(i_s-1)\alpha_s$
Rotor, *a*	$\theta_a(i_r,j_r)=(j_r-1)\beta+(i_r-1)\alpha_r+\varphi$
Stator, *B*	$\theta_B(i_s,j_s)=(j_s-1)\beta+(4q_s+i_s-1)\alpha_s$
Rotor, *b*	$\theta_b(i_r,j_r)=(j_r-1)\beta+(4q_r+i_r-1)\alpha_r+\varphi$
Stator, *C*	$\theta_C(i_s,j_s)=(j_s-1)\beta+(2q_s+i_s-1)\alpha_s$
Rotor, *c*	$\theta_c(i_r,j_r)=(j_r-1)\beta+(2q_r+i_r-1)\alpha_r+\varphi$

* $q_s \geq 1$, $q_r \geq 1$, $p_p \geq 1$. $1 \leq i_s \leq q_s$, $1 \leq i_r \leq q_r$, $1 \leq j_s, j_r \leq p_p$.

D. The Equivalent-Circuit Inductances

Finally, the winding inductance values are converted into the per-phase equivalent circuit values. The equivalent circuit of an ACRIM is shown in Fig. 4, where ω_s is the stator supply frequency, k is the stator-to-rotor turns ratio, s is the slip value, R_s, R_r are the stator and rotor per-phase resistance respectively, C_s and C_r are the stator and rotor capacitance respectively, L_s, L_r are the stator and rotor self-inductances respectively, L_m is the magnetizing inductance.

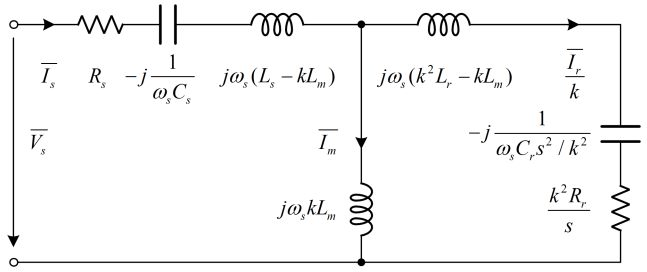

Fig. 4: Per-phase equivalent circuit of an ACRIM (motor convention).

The detailed derivation for winding inductance values has been given in [1], so only the final expressions are presented here. The stator and rotor self-inductance values used in the equivalent circuit are

$$L_s = \left|L_{sA} - M_{AB}\right|,\ L_r = \left|L_{ra} - M_{ab}\right| \tag{14}$$

where L_{sA} and L_{ra} are the self-inductance of stator phase *A* and rotor phase *a* winding respectively. The magnetizing inductance value used in the equivalent circuit is,

$$L_m = (M_{Aa}^2 + M_{Ab}^2 + M_{Ac}^2 - M_{Aa}M_{Ab} - M_{Ab}M_{Ac} - M_{Ac}M_{Aa})^{1/2} \tag{15}$$

which is applicable to any rotor position.

IV. 3-D FEA Results and Validation

For preliminary validation of the proposed analytic inductance calculation approach, a 3-D FEA model of a three-phase, six-pole air-cored IM was built in COMSOL. Single-layer fully-pitched coil windings were considered initially for the stator and rotor, with $q_s = 3$ and $q_r = 2$ coils per pole per phase for the stator and rotor respectively. Since simple rectangular or hexagonal coil shape would cause end-coil intersections in the full winding — which cannot be tolerated in a 3-D FE model — hexagonal coils with end-steps were adopted for the 3-D FE model, as shown in Fig. 5. The coil dimensions are given in Table VI and three snapshots of the 3-D FE winding models are shown in Fig. 6.

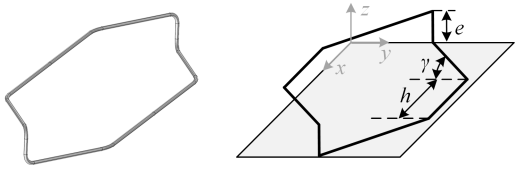

Fig. 5: The hexagonal coil used in the FE model (left) and the hexagonal coil model used in analytic calculation (right).

Table VI
Geometry of the Stator and Rotor Coils in the Six-Pole Machine.

	Stator	Rotor
Baseline circle radius, r_b	109.9 mm	103.3 mm
Conductor diameter, d_c	3.5 mm	3.5 mm
Length of the axial conductors, h	253.3 mm	200 mm
Step height, e	35 mm	24 mm
End-winding angle, γ	60°	43°
Number of coils per pole per phase, q	3	2

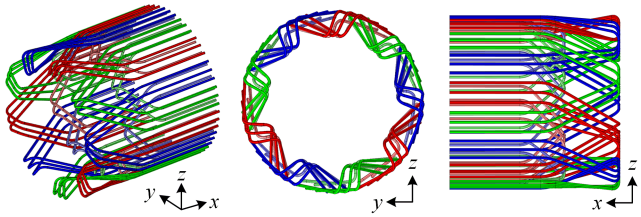

Fig. 6: The 3-D FE model for the stator and rotor windings.

The analytic and FEA results are compared in Table VII, where both results are calculated when stator phase *A* and rotor phase *a* are geometrically aligned, i.e., when the rotor position is $\varphi = (\alpha_r - \alpha_s)/2 = 1.67°$. The FE winding inductance values are all directly extracted from COMSOL, the FE values of the inductances used in the equivalent circuit are calculated based on the FE winding inductances. It can be seen that the largest error is about 1%. Such small disagreements between analytic and 3-D FE results are deemed to be caused by discrepancies in the analytic and FE geometries and residual errors in the FE solution. In fact, coils in the analytic calculation have sharp corners while coils in the FE model have round corners.

On a PC with an i7 CPU (3.20 GHz) and a 16 GB RAM, the simulation time for the FE model is 1 h 31 min, the time required to calculate all the analytic values in Table VII is only 0.18 s. It is clear that the proposed method greatly reduces the computational cost.

V. Experimental Validation

In this section, the proposed method is validated using a manufactured ACRIM prototype, the inductance is initially

estimated based on the prototype geometry, then the machine performance is calculated, both are compared with the experimental results.

Table VII
Comparison of the Analytic and FEA Results When the Stator Phase *A* and Rotor Phase *a* are Geometrically Aligned *.

		Analytic value (unit: μH)	FE value (unit: μH)	Error (%)
Winding inductance breakdown	L_{sA}	11.7733	11.7110	−0.53
	L_{ra}	4.2965	4.2614	−0.82
	M_{AB}	−1.8008	−1.8052	0.24
	M_{ab}	−0.4251	−0.4293	0.98
	M_{Aa}	3.5040	3.4914	−0.36
	M_{Ab}	−0.9679	−0.9649	−0.31
	M_{Ac}	−0.7579	−0.7616	0.48
Equivalent circuit inductances	L_s	13.5741	13.5162	−0.43
	L_r	4.7216	4.6907	−0.66
	M	4.3707	4.3582	−0.29

* This condition corresponds to a rotor position φ = 1.67° in Fig. 3(b).

A. Structure of the ACRIM prototype

The ACRIM prototype is shown in Fig. 7. Both stator and rotor have hand-wound, six-pole, three-phase, single-layer lap windings, and two coils per pole per phase. The stator housing and rotor hub are cast using epoxy resin which is more lightweight compared to electrical steels and has the advantages of eliminating iron losses and saturation issues. Since the rotor is no longer magnetic, holes can be cut to remove some materials for further mass reduction and better cooling. Coils are glued to the slotless stator and rotor structure. Retaining sleeves are molded outside the rotor end-windings to reduce deformation and avoid stator-rotor contact in rotation. For cooling enhancement, air is also blown into the prototype through pipes connected to the front cover. In this paper, the prototype has stator capacitors only so stator windings are connected to the supply inverter through capacitors in series and the rotor windings are short-circuited.

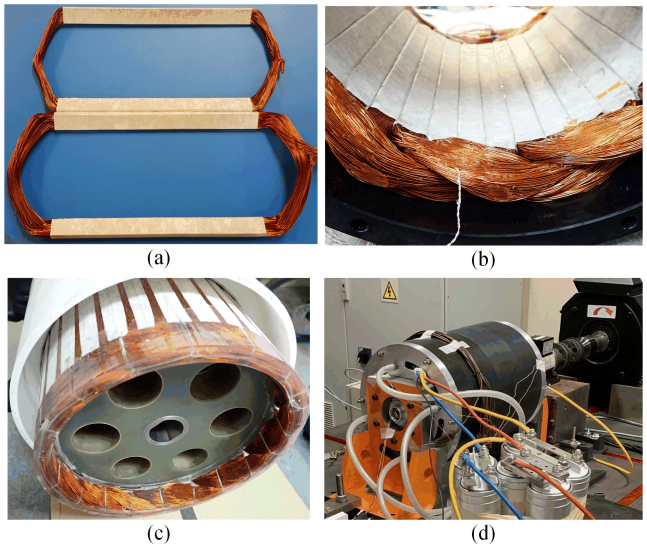

Fig. 7: Photos of the ACRIM prototype (a) pre-formed rotor coil (top) and stator coil (bottom) before mounting on the machine; (b) stator housing and coils; (c) rotor hub and coils; (d) assembled ACRIM prototype with capacitors.

B. Coil shape determination and analytic estimation

To estimate the inductances, the first step is to determine the analytic coil shape. Since coils are initially wound and pre-formed on a jig, then mounted and fixed to the epoxy stator housing or rotor hub one by one, all stator or rotor coils are assumed to be identical. It can be seen from Fig. 7b and Fig. 7c, the coil end-windings are arranged in a manner to avoid coil-to-coil clashing and the bundle of end-windings are bent along the stator or rotor periphery to avoid stator-to-rotor clashing. Fig. 8 sketches a sectional view of the ACRIM. In the manufacturing process, due to the overlaps in the coil ends, the end-winding region has a thicker radial depth than the axial region. To describe the shape of one coil end, the winding diagram of the stator and rotor is drawn as Fig. 9a, for the end-windings of coils in phase *A*, their left-edges can be seen on the top of the coils in phase *B* and their right-edges can be seen on the bottom of coils in phase *C*, and situations are the same for end-windings of phase *B* and phase *C* coils. This arrangement of the coil ends can be simplified and the displacement of coil ends in the radial direction can be lumped together and characterised by steps. As a result, the end-winding region can be seen to have two layers, each coil has half coil end in the top layer as plotted by solid lines in Fig. 9b and the other half end in the bottom layer as plotted by dashed lines. Fig. 10a shows one stator coil and one rotor coil with the two-layer end, their axial parts are on the baseline circles and are parallel to the *x*-axis. To avoid clashing in rotation, the stator coil ends are bent outwards forming a top layer and the rotor coil ends are bent inwards forming a bottom layer, while the stator bottom layer and the rotor top layer are on the stator and rotor baseline circles respectively. The two layers are connected by steps e_s and e_r. Fig. 10b shows a top view of the stator and rotor coils, their end-winding angles are γ_s and γ_r respectively.

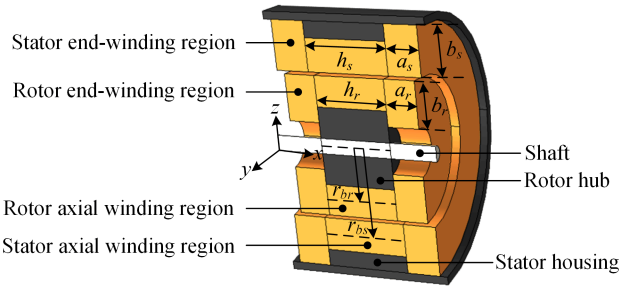

Fig. 8: A sectional view of the ACRIM.

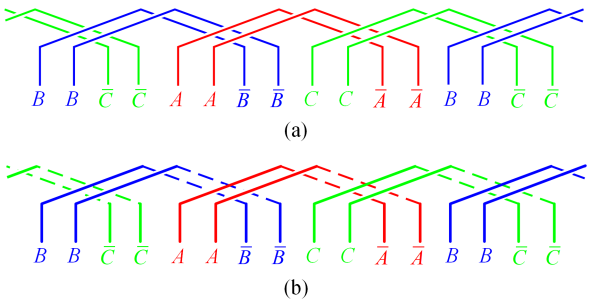

Fig. 9: (a) End-winding layout of the stator and rotor coils in the ACRIM prototype; (b) End-winding layout of the stator and rotor coils with the illustration of a two-layer arrangement in the end-winding region where solid lines represent the top layer and dashed lines represent the bottom layer.

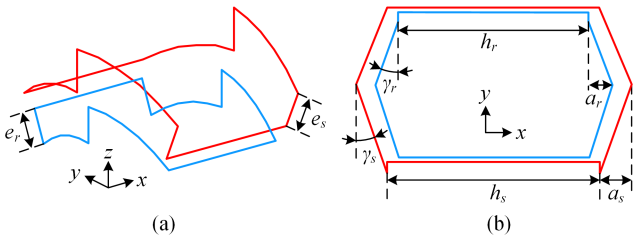

Fig. 10: Shapes of the stator (red) and rotor (blue) coils used in the analytic calculation (a) oblique view, (b) top (*xy*) view.

The measurable geometric parameters of the ACRIM prototype are collected in Table VIII. Based on the geometric relationship shown in Fig. 8 and Fig. 10, the step size is calculated as $e = b-d$, and are $e_s = 16.8$ mm and $e_r = 14$ mm for stator and rotor coils respectively, the end-winding angle is calculated as $\gamma = \tan^{-1}[(a-c/2)/(\pi r_b/6)]$, giving $\gamma_s = 27.85°$ and $\gamma_r = 25.67°$ for stator and rotor coils respectively. It is assumed that the coil-side area is constant over the coil, and equivalent round cross sections with the actual coil-side area are used in the analytic calculation. The curved coil ends are broken into several straight segments. The complete stator and rotor three-phase windings used in the analytic calculation are shown in Fig. 11. The calculation results are collected in Table IX.

Table VIII
Geometry of the ACRIM Prototype

	Stator	Rotor
Number of coils per pole per-phase, q	2	2
Axial winding baseline circle radius, r_b	109.9 mm	103.3 mm
Axial winding coil side radial depth, d	7.2 mm	3.5 mm
Axial winding coil side tangential width, c	19.2 mm	18.0 mm
Axial winding length, h	240 mm	215 mm
End-winding region axial length, a	40 mm	35 mm
End-winding region radial depth, b	24 mm	17.5 mm

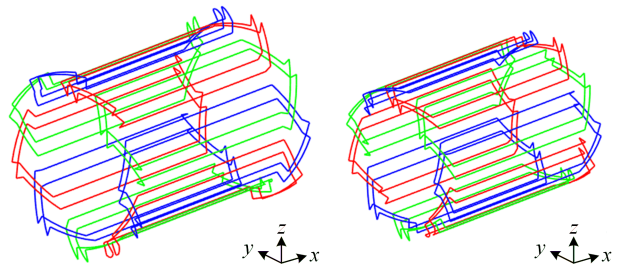

Fig. 11: Shapes of the stator (left) and the rotor (right) three phase windings used in the analytic calculation. Red, blue and green colors represent the three phases respectively.

C. Testing and results comparison

In the parameter testing, the phase winding resistance and phase self-inductance are directly measured using an LCR meter. The stator or rotor phase-to-phase mutual inductance is measured by energizing one stator or rotor phase using AC current and measuring the induced voltages in the other phases. The stator-to-rotor mutual inductances are measured in the same way when the stator and rotor are magnetically aligned, which is obtained by energizing stator phase *A* and carefully rotating the rotor to a position at which the maximum induced voltage is observed in rotor phase *a*. All the phase-to-phase mutual inductances, $M_{ph\text{-}ph}$, are calculated using $M_{ph\text{-}ph} = V/\omega I$, where I and ω are the excitation-current magnitude and frequency respectively, V is the induced-emf magnitude in the other winding. The measured values are collected and compared with the analytic estimations in Table IX. The discrepancies are calculated with respect to the test values.

As shown in Table IX, the discrepancies in resistances are around 3% which assure that the analytic coil shapes have a close total length as the prototype coil. The inductance values are very small, in the levels of hundreds of μH. The estimated values are all of the same orders of magnitude as the tested values and exhibit a reasonable degree of accuracy. Most of the discrepancies are within 10%. The major discrepancies are as follows: 33.87% discrepancy in the stator phase-to-phase mutual inductance, −16.53% in the stator-to-rotor aligned mutual inductance and 23.11% in the stator-to-rotor heteronym mutual inductance. There are several factors that may contribute to these discrepancies. Firstly, all coils are assumed to be identical in the analytic estimation, but the shapes of hand-wound coils in the prototype are likely to differ from coil to coil, especially at the coil ends. Secondly, the analytic coil shape is a simplification of the real shape, as it lumps the gradual displacement in the radial direction into steps and assumes a constant end-winding angle. Thirdly, analytic coils are assumed to have an unvarying, round cross-section, but the real coils have flatter cross sections and their shape change in the end-winding region.

For the ACRIM prototype with hand-wound windings, because of the manufacture uncertainties, the shapes, cross-sections and arrangement of end-windings are very complex and it is extremely difficult to build an accurate 3-D FE model – a "high-fidelity" 3-D FE model would require a very detailed set of in-situ 3D measurements on the individual coil shapes or even a 3D scanning. On the other hand, a 3-D FE model for the notional coil shape derived from the measured geometry in section V.B using real cross-sectional areas results in clashes in end-winding conductors which cannot be tolerated in the 3-D FE models as they prevent the definition of individual coils. To avoid clashing, the end-winding step size, angle or the cross-section area have to be varied but this causes deviations from the measured prototype geometry constraints, which makes the results no longer comparable. However, a "filamentary" 3-D FEA model which has the same winding shape as Fig. 11 and uses thin round wires with 2 mm radius rather than actual cross-sections to avoid conductor clashing can still be built to cross-check the estimated mutual inductance results, which are less sensitive to the coil-side cross-section shape. Clearly self-inductances are not comparable [23]. The 3-D FE model is shown in Fig. 12, the results are compared in Table IX. The discrepancies for estimated M_{AB}, M_{ab}, M_{Aa}, M_{Ab}, M values with respect to corresponding 3-D FEA results are 0.94%, 0.66%, −0.05%, 0.47% and 0.01% respectively. It can be seen that there is good agreement between the estimated and FEA values as demonstrated in the previous section for a different geometry.

In fact, in the proposed analytic approach, the real coil-side cross-section area can be taken into account even with the notional coil shapes derived from a few measurements on the prototype geometry (section V.B) and even if this process entails end-winding clashing. Unlike 3-D FEA, the proposed approach can handle conductor intersecting and resolve mathematical singularity issues, so it is very robust. In addition, the proposed method avoids highly-detailed modelling work, and achieves a reasonable degree of accuracy. Closed-form expressions and the inductance collection routine further accelerate its calculation speed, so it can be integrated into an optimization program.

Table IX
Comparison of the Analytic Estimated,
"Filamentary" 3-D FEA and Test Values

	Estimated value	"Filamentary" 3-D FEA value	Measured value	Discrepancy * (%)
R_s (mΩ)	200.75	/	198.20	−1.29
R_r (mΩ)	381.47	/	393.93	3.16
L_{sA} (μH)	712.47	/	661.25	−7.75
L_{ra} (μH)	669.48	/	628.10	−6.59
M_{AB} (μH)	−56.49	−57.03	−85.43	33.87
M_{ab} (μH)	−59.88	−60.27	−63.99	6.44
M_{Aa} (μH)	482.31	482.06	413.89	−16.53
M_{Ab} (μH)	−62.61	−62.91	−81.43	23.11
L_s (μH)	768.96	/	746.68	−2.98
L_r (μH)	729.36	/	692.09	−5.38
M (μH)	544.92	544.97	495.32	−10.01

* The "Discrepancy" refers to the discrepancy of estimated values with respect to measured values.

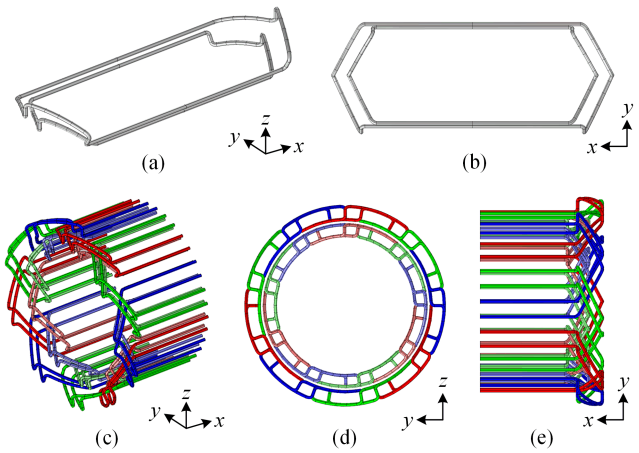

Fig. 12: The 3-D FE model for prototype-inductance validation, (a) and (b) show one stator coil and one rotor coil; (c), (d) and (e) show the stator and rotor windings.

The ultimate goal of inductance calculations is the ACRIM performance prediction. Therefore, the ACRIM performance predicted by using the equivalent circuit with analytic estimated and tested R, L values in Table IX were also compared with the performance at the test-bench. In the first experiment, because of heating issues and mechanical speed limitations, the ACRIM prototype is operating under a 10 Vrms, 150 Hz AC voltage supply with the rotor speed varying from 0 to 3000 rpm. Fig. 13 shows test results for the ACRIM with and without (i.e., a simple air-cored IM — "ACIM") capacitors. The ACRIM stator capacitance is 1.653 mF per phase, tuned to cancel out the equivalent reactance seen from the ACIM stator terminals at the peak-efficiency slip, i.e., the ACRIM achieves unity power factor at its peak-efficiency point under this supply frequency [4]. The torque is also improved since the stator winding is carrying more current compared with the ACIM. It can be seen that the machine torque, efficiency and power factor versus slip curves predicted using estimated R, L show good corelations with the test points. However, there is an overestimation in the efficiency. The difference between the two efficiency-slip curves plotted using measured and estimated R, L is larger than 3% in the slip range of 0.080 to 0.297 and the largest difference is 3.59% at the slip of 0.16. This is caused by the assumption of round cross-section coils in the mutual inductance calculation, which are explained in detail in a later paragraph.

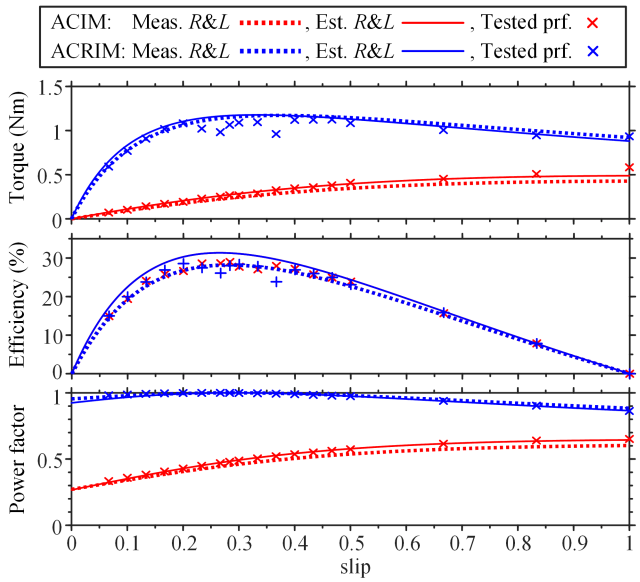

Fig. 13: Comparison of the torque, efficiency and power factor versus slip curves calculated using measured R, L values (Meas. R&L), and using analytic estimated R, L values (Est. R&L), with tested points (Tested prf.) of the ACRIM with 1.653 mF stator capacitor at 10 Vrms, 150 Hz voltage supply.

Another experiment was carried out to validate the performance prediction accuracy under different frequencies. The capacitance of the ACRIM per phase was 900 μF, the stator supply AC current magnitude and the rotor speed were held constant at 30 Apk and 2800 rpm respectively while the supply frequency was varied from 150 Hz to 300 Hz. In Fig. 14, the torque, efficiency and power factor versus supply frequency curves calculated using measured and estimated R, L values were compared to the tested points. Again, good agreement was observed between the estimated and tested curves. Using the analytic estimated R, L values, the power factor becomes unity when the supply frequency was 223 Hz, and the tested unity power factor point occurs at a supply frequency of 220 Hz.

The overestimation of efficiency (in Fig. 13) and torque (in Fig. 14) was mainly caused by the overestimation of the magnetizing inductance. It is known that the mutual

inductance between two conductors with round cross sections is sensibly the same as the mutual inductance between their central filaments [23]. However, applying this principle to conductors with non-infinitesimal, non-circular cross-sections can lead to an overestimation in mutual inductance. In the prototype, the axial portion of the coil sides have a flatter cross-section shape. A hybrid method combining the proposed filament-based method with a 2-D FEA modeling the real cross section shape of the axial coil sides can be used to correct the self and mutual inductances of axial parts. Though this increases the computational costs but it is still faster than a 3-D FEA. In addition, accurate representation of the actual 3-D coil shape including the inevitable manufacturing uncertainties like variations in end-winding cross-section shape and deviations to avoid end-winding clashing in a 3-D FEA might not be viable — especially for hand-wound windings, which may make the 3-D FEA results not fully representative for the real prototype.

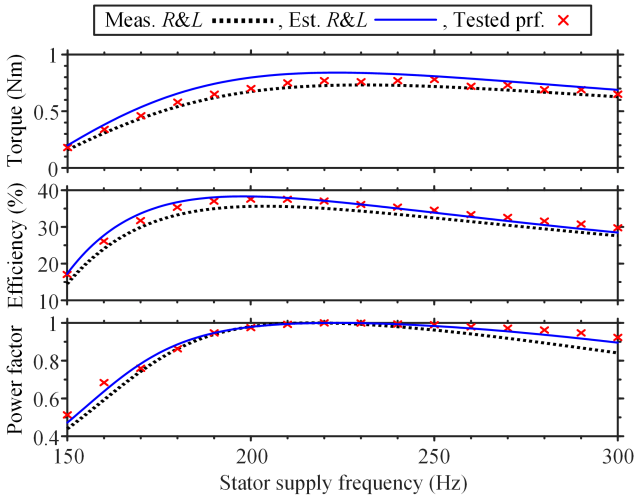

Fig. 14: Comparison of the torque, efficiency and power factor versus stator supply frequency curves calculated using measured *R*, *L* values (Meas. *R*&*L*), and using analytic estimated *R*, *L* values (Est. *R*&*L*), with the tested points (Tested prf.) of the ACRIM with 900 μF stator capacitor per-phase at 30 Apk AC current supply and constant rotor speed of 2800 rpm.

VI. Conclusion

This paper proposes a fast winding inductance estimation method for ACRIMs. The method uses closed-form expressions of Neumann integrals to calculate the basic inductance "module", i.e., self and mutual inductances of straight conductors placed at any orientation, and builds expressions for the self and mutual inductances of coils composed by these straight conductors. A collection routine for phase-winding self and mutual inductances is developed, including the mutual inductance between any stator and rotor phase windings at a generic rotor position, which is useful in torque ripple estimation. The number of calculations is limited to a minimum by considering only independent coil pairs. Finally, the self-inductances and magnetizing inductance used in the equivalent circuit are derived so that the machine operating characteristics can be calculated. Compared to 3-D FE models, the proposed analytic approach has a significantly lower computational burden and allows coil intersections to be handled automatically without raising singularity issues. The validation against a 3-D FE model shows that the analytic estimation method achieves a very good accuracy. The proposed method is also validated experimentally on a purposely-built ACRIM prototype: a full coil shape parametric representation based on measurable geometric parameters is presented, and reasonable accuracy is confirmed in the comparison between estimated and tested equivalent-circuit inductances, with a maximum discrepancy of about 10%. However, it is worth remarking that the estimation accuracy has a high dependency on the modelling accuracy of the real coil shape, and a high-fidelity coil shape representation for "manually-wound" prototype coils is difficult so higher discrepancies up to 33.87% can be found in some of the winding inductance breakdown values. Finally, the ACRIM performance predicted using estimated inductances is compared with experimental tests, which shows a good correlation.

Appendix

The expressions of terms *S*, *Z*, *K* in (9) for the summation of mutual inductances between coils in the same phase but different pole pairs are presented below.

$$S(j)=\begin{cases} qM(j\beta)+\sum_{i=1}^{q-1}(q-i)M(j\beta\pm i\alpha) & \text{if } q\geq 2 \\ M(j\beta) & \text{if } q=1 \end{cases} \tag{16}$$

$$Z=\begin{cases} S(\frac{p_p}{2}) & \text{if } p_p\geq 2 \text{ and } p_p \text{ is even} \\ 0 & \text{if } p_p\geq 3 \text{ and } p_p \text{ is odd} \end{cases} \tag{17}$$

and

$$K=\begin{cases} \frac{p_p-1}{2} & \text{if } p_p\geq 3 \text{ and } p_p \text{ is odd} \\ \frac{p_p}{2}-1 & \text{if } p_p\geq 4 \text{ and } p_p \text{ is even} \end{cases} \tag{18}$$

References

[1] Z. Jin *et al.*, "Winding Inductance Estimations in Air-Cored Resonant Induction Machines," in *Proc. IEEE Energy Convers. Congr. Expo.*, 2020, pp. 5813-5820.

[2] Y. Fujimoto, "Modeling and analysis of wireless electro-mechanical energy transfer and conversion using resonant inductive coupling," in *Proc. 41st Annu. Conf. IEEE Ind. Electron. Soc.*, 2015, pp. 004905-004910.

[3] Z. Jin, M. F. Iacchetti, A. C. Smith, R. P. Deodhar, and K. Mishima, "Comparison of different capacitor tuning criteria in air-cored resonant induction machines," in *Proc. IEEE Energy Convers. Congr. Expo.*, 2019, pp. 3017–3024.

[4] Z. Jin *et al.*, "Air-Cored Resonant Induction Machines: Comparison of Capacitor Tuning Criteria and Experimental Validation," in *IEEE Trans. Ind. Appl.*, vol. 57, no. 4, pp. 3595-3606, July-Aug. 2021.

[5] M. F. Iacchetti, R. P. Deodhar, A. C. Smith and K. Mishima, "Modelling and Operating Characteristics of Air-Cored Resonant Induction Machines," in *Proc. IEEE Energy Convers. Congr. Expo.*, 2018, pp. 6468-6475.

[6] B. J. Ebot and Y. Fuiimoto, "A General Framework for the Analysis and Design of a Wireless Resonant Motor," in *Proc. IEEE Int. Elect. Mach. Drives Conf.*, 2019, pp. 1966-1970.

[7] K. Sakai and K. Takijima, "Basic Characteristics of an Ultra-Lightweight Magnetic Resonance Coupling Motor with Various

Numbers of Poles," in *Proc. IEEE Energy Convers. Congr. Expo.*, 2018, pp. 7342-7348.
[8] M. Liu, K. W. Chan, J. Hu, Q. Lin, J. Liu and W. Xu, "Design and Realization of a Coreless and Magnetless Electric Motor Using Magnetic Resonant Coupling Technology," in *IEEE Trans. Energy Convers.*, vol. 34, no. 3, pp. 1200-1212, Sept. 2019.
[9] A. Taieb Brahimi, A. Foggia and G. Meunier, "End winding reactance computation using a 3D finite element program," in *IEEE Trans. Magn.*, vol. 29, no. 2, pp. 1411-1414, March 1993.
[10] R. Lin and A. Arkkio, "Calculation and Analysis of Stator End-Winding Leakage Inductance of an Induction Machine," in *IEEE Trans. Magn.*, vol. 45, no. 4, pp. 2009-2014, April 2009.
[11] K. Takeuchi, M. Matsushita, H. Makino, Y. Tsuboi and N. Amemiya, "Finite-Element Analysis for Magnetic Flux in End Region of Synchronous Machine Using End-Winding Model," in *IEEE Trans. Magn.*, vol. 57, no. 2, pp. 1-6, Feb. 2021, Art no. 7400506.
[12] Z. Zhang, A. Matveev, R. Nilssen and A. Nysveen, "Ironless Permanent-Magnet Generators for Offshore Wind Turbines," in *IEEE Trans. Ind. Appl.*, vol. 50, no. 3, pp. 1835-1846, May-June 2014.
[13] Y. Huang, B. Ge, J. Dong, H. Lin, J. Zhu and Y. Guo, "3-D Analytical Modeling of No-Load Magnetic Field of Ironless Axial Flux Permanent Magnet Machine," in *IEEE Trans. Magn.*, vol. 48, no. 11, pp. 2929-2932, Nov. 2012.
[14] L. Urankar, "Vector potential and magnetic field of current-carrying finite arc segment in analytical form, Part III: Exact computation for rectangular cross section," in *IEEE Trans. Magn.*, vol. 18, no. 6, pp. 1860-1867, November 1982.
[15] F. Maurer, B. Kawkabani and J. K. Nøland, "Rapid 3-D Magnetic Integral Field Computation of Current-Carrying Finite Arc Segments with Rectangular Cross Section," in *IEEE Trans. Magn.*, vol. 56, no. 2, pp. 1-12, Feb. 2020, Art no. 8100312.
[16] F. Maurer and J. K. Nøland, "A Rectangular End-Winding Model for Enhanced Circulating Current Prediction in AC Machines," in *IEEE Trans. Energy Convers.*, vol. 36, no. 1, pp. 291-299, March 2021.
[17] A. Smith and S. Williamson, "End-winding leakage reactance of concentrically-wound machines," in *Proc. 15th Int. Conf. Electr. Mach.*, 2002, pp. 64–69.
[18] D. Ban, D. Zarko and I. Mandic, "Turbogenerator end-winding leakage inductance calculation using a 3-D analytical approach based on the solution of Neumann Integrals," in *IEEE Trans. Energy Convers.*, vol. 20, no. 1, pp. 98-105, March 2005.
[19] C. Ye, K. Yu, G. Zhang and Y. Pan, "The Windings Inductance Calculation of an Air-Core Compulsator," in *IEEE Trans. Magn.*, vol. 45, no. 1, pp. 522-524, Jan. 2009.
[20] A. Tessarolo, "Computing end-turn leakage inductance of concentric coil windings by asymptotical series approximation of Neumann integrals," in *Proc. XIX Int. Conf. Electr. Mach.*, 2010, pp. 1-6.
[21] M. Bortolozzi, A. Tessarolo and C. Bruzzese, "Analytical Computation of End-Coil Leakage Inductance of Round-Rotor Synchronous Machines Field Winding," in *IEEE Trans. Magn.*, vol. 52, no. 2, pp. 1-10, Feb. 2016, Art no. 8100310.
[22] R. A. Howard, Y. Xiao and S. D. Pekarek, "Modeling and Design of Air-Core Tubular Linear Electric Drives," in *IEEE Trans. Energy Convers.*, vol. 28, no. 4, pp. 793-804, Dec. 2013.
[23] F. W. Grover, *Inductance calculations: working formulas and tables*. Courier Corporation, 2004.

Zhao Jin received the B.Eng. degree in electrical engineering and automation from the University of Electronic Science and Technology of China, Chengdu, China, in 2017, and the M.Sc. degree in power electronics, machines, and drives from the University of Manchester, Manchester, U.K., in 2018, where he is currently working toward the Ph.D. degree in electrical engineering. He was a Visiting Student with the University of Michigan-Dearborn, Dearborn, MI, USA, from 2016 to 2017. His research interests include design and modeling of electric machines.

Matteo F. Iacchetti (Senior Member, IEEE) received the Ph.D. degree in electrical engineering from the Politecnico di Milano, Milan, Italy, in 2008. From 2009 to 2014, he has been a Postdoctoral Researcher with the Department of Energy at Politecnico di Milano. He is currently a Senior Lecturer with the Department of Electrical and Electronic Engineering, University of Manchester, Manchester, U.K., and an Associate Professor with the Department of Energy at Politecnico di Milano, Milan, Italy. His main research interests include design, modeling, and control of electrical machines and drives.

Alexander C. (Sandy) Smith (Senior Member, IEEE) received the B.Sc. (Eng) and Ph.D. degrees from Aberdeen University, Aberdeen, U.K., in 1977 and 1980, respectively, both in electrical engineering. Previous academic appointments with Imperial College, London, U.K., and Cambridge University, Cambridge, U.K. Joined Invensys Brook Crompton, Huddersfield, U.K., in 1997 as the Head of Research for motor technology and now a Professor of Electrical Machines with the University of Manchester, Manchester, U.K. and the Director of the Roll-Royce University Technology Centre on Electrical Systems for Extreme Environments. His research interests include design and modeling of motors, generators, superconducting machines, and electrical drive systems.

He is a Fellow of the Institute of Engineering and Technology, and previously the Editor-in-Chief of the *IET Journal Electrical Systems in Transportation*.

Rajesh P. Deodhar (Senior Member, IEEE) received the B.Eng. degree from the University of Mumbai, Mumbai, India, in 1989, the M.Tech. degree from CEDT, Indian Institute of Science, Bangalore, India, in 1991, both in electronics engineering, and the Ph.D. degree in electrical engineering from the University of Glasgow, Scotland, U.K., in 1996.

He has had work experience with Crompton Greaves Ltd. of India, Hitachi Ltd., Tokyo, Japan, and SPEED Laboratory, University of Glasgow, Glasgow, U.K. In 1998, he joined IMRA Europe S.A.S. U.K. Research Centre, Brighton, U.K., where he currently serves as a Research Specialist working on the design and analysis of a wide range of motors and actuators used in automotive components and systems. He is a co-author for over one hundred publications at international conferences and peer-reviewed journals, including being a named co-inventor for over 40 international patent (applied or granted) documents.

Dr. Deodhar has received numerous awards, including the IISc Gold Medal in 1991, the IAS Electric Machines Committee first prize paper Award in 1996, the IEEE T-IA journal second prize paper Award in 1998 and 2017, as well as best paper awards at various IEEE international conferences in 2010, 2012, and 2014. He serves as a reviewer for a number of IEEE journals, and as a TPC member for a number of international conferences, and, is a past Associate Editor for the IEEE T-IA journal. He is a Chartered Engineer and a Fellow of the Institution of Engineering and Technology in the U.K..

Yoshiyuki Komi (Member, IEEE) received the B.Sc. degree in mechatronics engineering from Wakayama University, Wakayama, Japan, in 2007. He joined Suzuki Motor Co. in 2007 and worked on ICE and electric motors. In 2013, he joined Aisin Seiki Co. Kariya, Japan, and he is currently working as a Research Engineer with IMRA Europe U.K. Research Centre, Brighton, U.K. His research interests include development of high power density motors and actuators.

Ahmad Anad Abduallah (Student Member, IEEE) received the B.Sc. and M.Sc. degrees in electrical engineering from Qatar University, Doha, Qatar, in 2012 and 2015, respectively. He is working toward the Ph.D. degree in electrical engineering with Liverpool John Moores University, Liverpool, U.K. Since 2016, he has been with Liverpool John Moores University. From 2012 to 2015, he was a Research Assistant and Associate with Qatar University. He is currently working as a Research Engineer with Institut Minoru de Recherche Avancée (IMRA) Europe research Centre, Brighton, U.K. His research interests include power electronics and advanced machine drives.

Chiaki Umemura received the B.Sc. degree in engineering physics from the University of Tsukuba, Tsukuba, Japan, in 1987. In 1987, he joined Aisin Seiki Co., Ltd. Kariya, Japan. Since 2018, he is the General Manager of U.K. Research Centre, IMRA Europe S.A.S., Brighton, U.K. His research interests include developing high power density motors and actuators.